water

MDPI

Article

Characterization of Flowpath Using Geochemistry and $^{87}Sr/^{86}Sr$ Isotope Ratios in the Yalahau Region, Yucatan Peninsula, Mexico

Jessica McKay [1,2], Melissa Lenczewski [1,*] and Rosa Maria Leal-Bautista [3]

1 Department of Geology and Environmental Geosciences DeKalb, Northern Illinois University, DeKalb, IL 60115, USA; jmckay@tamu.edu
2 Department of Geology and Geophysics, Texas A&M University, College Station, TX 77843, USA
3 Centro de Investigacion Cientifica de Yucatan, Unidad de Ciencias del Agua, Cancun, Quintana Roo 77524, Mexico; rleal@cicy.mx
* Correspondence: lenczewski@niu.edu; Tel.: +1-815-762-5452

Received: 12 August 2020; Accepted: 11 September 2020; Published: 16 September 2020

Abstract: The Yalahau region, located in the northeastern portion of the Yucatán Peninsula, hosts a series of elongated depressions trending north/south in the direction of Isla Holbox, identified as the Holbox Fracture Zone. Previous studies have explored the geomorphology and various hydrologic characteristics of the Yucatán Peninsula; however, there is a paucity of data concerning the interior region where the fractures are located. Strontium isotope ratios and major ion geochemistry data of the surface water and groundwater of this region serve as a hydrogeochemical fingerprint, aiding in constraining the hydrological boundaries, determining flow paths, and characterizing hydrogeochemical processes that impact the composition of the groundwater within the region. $^{87}Sr/^{86}Sr$ isotope ratios indicate a different signature than the surrounding bedrock Sr ratio, suggesting that the flow throughout the Yalahau region is moving through channels faster than that of much of the Yucatán. Through major ion geochemistry and $^{87}Sr/^{86}Sr$ isotope ratios, we were able to delineate at least two flow paths within the Yalahau region and identify a point of saline intrusion at least 35 km from the coast. Gaining an understanding of the hydrogeochemistry and water flow regions is crucial in determining the impact of various activities (e.g., extensive tourism, drinking water withdrawal, wastewater discharge/injection) that occur within the Yucatán Peninsula.

Keywords: geochemistry; $^{87}Sr/^{86}Sr$ isotope ratios; flow path; Yucatan Peninsula

1. Introduction

The Yalahau region, located in the northeastern portion of the Yucatán Peninsula (YP), contains a series of elongated solution depressions filled with water trending north/northeast in the direction of Isla Holbox, identified as the Holbox Fracture Zone [1]. The wet swales and depressions are locally identified as "sabanas" and were first delineated using remote sensing [2,3]. The most prominent sabanas of the Holbox Fracture Zone lie within the northern 50 km of the fracture zone within the Mayan Northern Lowlands Yalahau region [4]. Sabanas extend approximately 100 km, trending NE-SW, ending near the city of Coba in the SW [5] and Holbox in the NE (Figure 1). The sabanas follow a lineament system that is probably linked to an underlying fault system. Previous studies [5–9] have explored the geomorphology and various hydrologic characteristics of the Yucatán Peninsula; however, there is a paucity of data concerning the northeastern interior where the Holbox Fracture Zone is located.

Water **2020**, *12*, x FOR PEER REVIEW 2 of 15

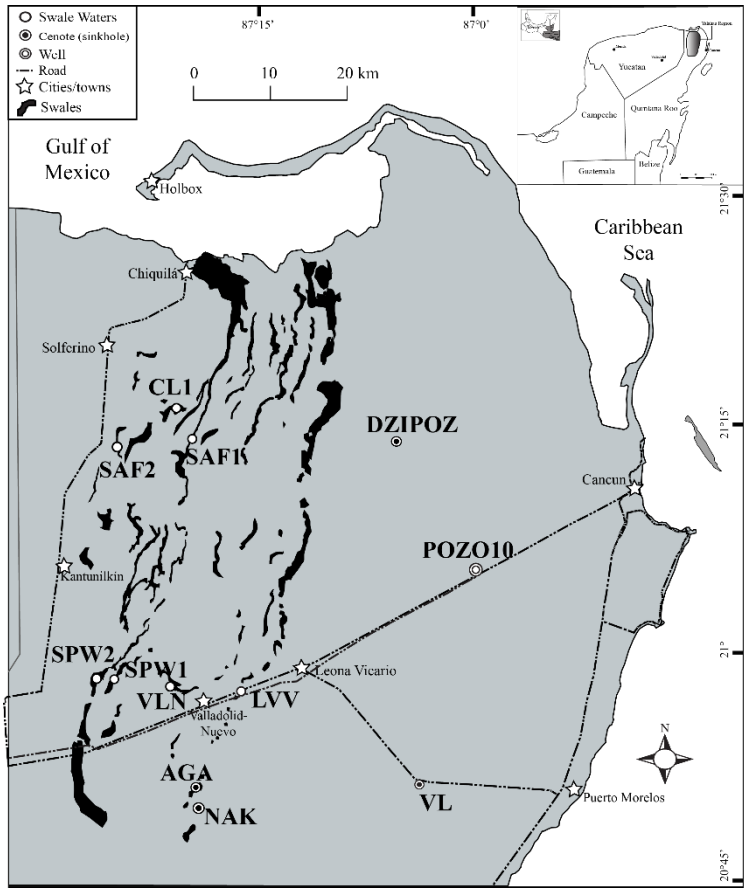

Figure 1. *Yalahau region site map showing sampling points.*

The Yalahau region is rich in Mayan history, containing a significant number of archeological sites [10,11]. The network of sabanas (or elongated linear depressions [12]) makes the region particularly unique in the Northern Yucatán. As there are no rivers in this region, the sabanas allow for easy access to freshwater without having to drill into the aquifers. The existence of many Mayan excavation sites along the exterior of the fracture zone suggests that sabanas served as a hub for many Mayan villages. Currently, much of the Yalahau region is remote, except for a few, small villages and the increasingly popular tourist destination of Holbox Island on the northern coast [13].

Hydrogeological characteristics of the Yalahau region have not been studied in detail in the past. While previous studies [6,7,14] have inferred flow patterns and geochemistry of the surrounding area; however, questions still remain regarding the movement of water through the fracture zone [14]. Other studies on geochemical and physical hydrological data lack sample points located within the fracture zone [5–7,15–17]. There have been some studies in the southern area of the region near Tulum using remote sensing [18,19]. The scarcity of available literature and data can be attributed to poor accessibility, heavy vegetation, and focused interest on coastal areas of the region. However, increasing land development within Northeastern Yucatán and upgrades in technology have allowed for extended accessibility into areas of the Yalahau.

Unlike most groundwater studies that analyze groundwater quality after obtaining extensive knowledge of the subsurface geology to further define groundwater flow paths and hydrogeologic units, this study utilizes groundwater geochemistry in combination with $^{87}Sr/^{86}Sr$ to assist in the initial mapping of the subsurface. Specifically, this study utilizes a geochemical and isotopic approach to determine the sources and movement of groundwater flow paths within the region.

Groundwater chemistry in coastal areas is controlled predominantly by marine influences through seawater intrusion and water–rock interactions [20,21]. Previous work has shown the usefulness of major ion geochemistry analysis in understanding groundwater movement and rock–water interaction within the Yucatán aquifer [16,22–24]. This study helps to elucidate factors controlling the hydrogeochemistry in waters flowing through the Holbox Fracture Zone in the

of major ion geochemistry analysis in understanding groundwater movement and rock–water interaction within the Yucatán aquifer [16,22–24]. This study helps to elucidate factors controlling the hydrogeochemistry in waters flowing through the Holbox Fracture Zone in the Yalahau region. Specifically, by using the major ion geochemistry and physical chemical parameters to determine the influences of seawater intrusion and rock–water interaction on the geochemical composition of the water, in combination with strontium isotope geochemistry, this study also helps to further delineate varying flow paths throughout the region.

Strontium isotopes have proven to be effective as a natural tracer, used to understand flow patterns within an aqueous system and hydrogeochemical processes in aquifers in a region [25–32]. In this study, we utilize the $^{87}Sr/^{86}Sr$ isotopic ratios, where ^{87}Sr is radiogenic and derives from the beta decay of ^{87}Rb, and ^{86}Sr is non-radiogenic [33]. The $^{87}Sr/^{86}Sr$ ratio in a rock will increase with rates proportional to its Rb/Sr ratio and decay constant of ^{87}Rb. Chemical weathering of rocks releases strontium into the solution in groundwater, whose isotopic composition depends upon the geologic ages and Rb/Sr ratios of rocks contributing to the system [34]. Within an aquifer, groundwater will reflect the distinctive strontium signature of the host rocks along the flow paths [35]. Once waters reach the surface, the original $^{87}Sr/^{86}Sr$ ratio should remain unless waters are mixed with waters of a different isotopic composition. $^{87}Sr/^{86}Sr$ ratios are particularly useful because they are not fractionated by geochemical reactions, meaning that differences in isotope ratios are reflective of primarily mixing processes [29,31].

The objective of this research study in the Northern Yucatán Peninsula is to gain an understanding of the waters in the Yalahau region. This study will (1) characterize the hydrogeochemistry of water within the Yalahau region, (2) determine potential preferential paths of flow within the Yalahau region, and (3) constrain hydrological and hydrogeological boundaries of water flowing through the Holbox Fracture Zone. Identifying the flow path pattern is crucial in expanding our aqueous geochemical knowledge of the Yucatán Peninsula and essential in beginning to understand how development could potentially impact the region.

1.1. Study Area

This study will refer to the northern 50 km of the Holbox Fracture Zone, where sabanas are extensive, covering around 134 km^2 as the Yalahau region [4]. Northern Yucatán is typically very flat, with elevations not exceeding 25 m above mean sea level [5]. Sabana elevations within the Yalahau typically fall between −10 and 0 m amsl, while elevations of areas surrounding sabanas are approximately 5–15 amsl [8]. Accordingly, with Glover et al. [36], the Yalahau region is characterized by an abundance of rainfall, nearly twice the amount of rainfall that the rest of the Northern Peninsula receives (an average of 1276 mm annually [37]). These heavy rainfalls likely contributed to the formation of the sabanas that characterize this area of the Yucatán [11].

1.1.1. Climate

The Yalahau region is characterized by wet and dry seasons. The wet season will typically begin in late May, lasting until mid-December, while the dry season will begin in December and last into the spring months. This region can experience annual rainfall of up to 1500–2000 mm [9,38], much higher than other regions of the Yucatán that receive as little as 500 mm annually [10]. This likely contributed to the formation of the extensive sabanas in the area. The increased amount of rainfall can be attributed to the "double sea breeze effect" that occurs due to the meeting of the Gulf of México and Caribbean Sea winds [9]. Average temperatures in the region range from 23 to 29 °C [39].

1.1.2. Geology and Hydrogeology

The soluble carbonate platform of the Yucatán (Figure 1) hosts one of the most expansive karst aquifers in the world, expanding over 165,000 km^2 [14]. Through dissolution and fracturing of the soluble limestone bedrock, sinkholes (locally referred to as cenotes) and an extensive underground cave system have become widespread throughout the Yucatán Peninsula, specifically in the northeast.

The karstic nature of the surface rock allows rain to infiltrate into the groundwater quickly, where it collects and forms a layer of freshwater that sits on top of an intruding saline water layer, essentially making surface water scarce throughout the Yucatán [40]. This makes the Yalahau region unique, as the sabanas provide a freshwater source without tapping into the aquifer. Other notable features throughout the Yucatán that have the potential to affect groundwater movement, excluding the Holbox Fracture Zone, include the Ring of Cenotes, which is a permeable zone forming a semicircular band of cenotes around the Chicxulub Sedimentary Basin and the Ticul Fault Zone [41]. While much is unknown about the formation of the fractures and depressions that make up the Holbox Fracture Zone, there are a few speculations. The Holbox-Xel-Há fracture zone is a regional feature in the karst terrain of Northeastern Yucatan consisting of more than 100 km of long chains of elongated solution depressions where the sabanas are located [12].

The curvature and the southern extension of the sabanas parallel the regional gravity signature that possibly suggests a connection to the Chicxulub impact structure [12]. It is also possible that the alignment of fractures could be associated with offshore tectonic structures related to active plate boundaries in the Late Eocene [5]. Stratigraphically, there is not much variation with the rest of the Yucatan Peninsula. According to Weidie [1], this part of the YP is made up of carbonates that were deposited in the Pleistocene due to the transgression of the sea and which extend to a distance of 10 km inland. The exposed rock is in a range of ages ranging from the Late Cretaceous to the Holocene [1], with a trend of younger carbonates deposited on the margins, forming strata that are almost horizontal throughout the peninsula [42,43]. The best-known hydrogeological model of the aquifer indicates that coastal areas have the effect of saline intrusion, with a freshwater lens floating over the higher density salt water, which gives rise to the formation of halocline [44].

Groundwater in much of the Yucatán is typically classified as being slow moving, obtaining its ion chemistry from minerals that compose local aquifer rock. However, water in fast-flowing systems such as the Ring of Cenotes, and, hypothetically, the Holbox Fracture Zone, are likely to possess chemical characteristics of their source region, making geochemical studies of the waters useful as a tracer [7].

The Yucatán's carbonate characteristics affect the groundwater geochemistry due to the soluble minerals including calcite ($CaCO_3$), dolomite ($CaMg(CO_3)_2$), gypsum ($CaSO_4 \cdot 2H_2O$), and celestite ($SrSO_4$). Nearly all fresh groundwater samples of the Yucatán are at or close to saturation equilibrium with calcite and dolomite [16]. In an aquifer system dominated by carbonate rocks, this is expected. The presence of high compositions of sulfate (SO_4^{2-}) in waters would suggest interaction with evaporite beds that have been reported in exclusive areas within the Yucatán. These include gypsum-bearing deposits in Southern Quintana Roo [42] and gypsums/anhydrite from impact breccia associated with the Chicxulub Crater [45]. The presence of high-sulfate waters flowing through areas in the Ticul Fault Zone [6] has shown significant implications for tracing groundwater movements through the Yucatán utilizing ion geochemistry.

2. Materials and Methods

2.1. Water Sample Collection

Groundwater (at cenotes) and surface water samples (at sabanas) were 12 in total. Sabana samples (CL1, SAF1 and 2, SPW 1 and 2, VLN) were collected from the shore in undisturbed water locations. Cenote samples (LVV, AGA, NAK, VL, PZIPOZ) were collected using a Beta Van Dorm Wildco water sampler (Yulee, FL, USA). Water samples were collected for major ions, strontium, and $^{87}Sr/^{86}Sr$ isotopes at sites within the Yalahau region that lie in Holbox Fracture Zone over a five-day period in July of 2018 (wet season). Sampling of sabanas was avoided when there were significant rainfall events within 48 h. Samples from cenotes were collected during the dry season (January 2019) only due to the sabanas site being dried out. Sites were chosen based on accessibility and location along sabanas within the Holbox Fracture Zone. Two sites were selected outside of the fracture zone to serve as control points (VL, POZO10). Control points were chosen because they were in the coastal aquifer

system but close to sampling sites for this research project. All samples were immediately placed in a cooler and stored at 4 °C until analysis.

2.2. Physiochemical Properties

A HACH HQ 40d multi-probe (Loveland, CO, USA) was used to measure physio-chemical properties in the field for pH, temperature (°C), electrical conductivity (EC) (µS/cm), dissolved oxygen (DO) (mg/L), and oxidation-reduction potential (ORP) (mV). A plastic beaker was rinsed three times with sample water prior to measurements. Probes were calibrated regularly according to instructions of the manufacturer.

2.3. Major Ion Geochemistry

Water samples for major ion analysis were transported and stored in sterile, polypropylene 50 mL centrifuge tubes rinsed 3× with sample water. Ion samples were filtered in the field using 0.2 µm syringe filters. Major ion analyses were conducted on a Dionex Ion Chromatography System (IC; Waltham, MA, USA) at Northern Illinois University (NIU). Samples were analyzed for major cations including sodium (Na^+), potassium (K^+), Calcium (Ca^{2+}), magnesium (Mg^{2+}), ammonium (NH^{4+}), and lithium (Li^+) and major anions including fluoride (F^-), chloride (Cl^-), nitrate ($NO_3{}^-$) phosphate ($PO_4{}^{3-}$), and sulfate ($SO_4{}^{2-}$). Alkalinity was measured by digital titrations using HACH digital titrator on 50 mL of sample with 1.6 N H_2SO_4.

2.4. Strontium

Samples for strontium isotope and ion analysis were stored in acid-washed polypropylene 50 mL centrifuge tubes and preserved with ultrapure HNO_3 to a concentration of 0.005%. All samples were filtered from 0.2 µm syringe filters. Strontium ion concentrations were measured using inductively coupled plasma-atomic emission spectrometry (ICP-AES), EPA Method 6010C, at First Environmental Laboratory (Naperville, IL, USA). Strontium isotope ($^{87}Sr/^{86}Sr$) analyses were conducted at the University of Texas Austin using a Finnigan-MAT 261 thermal ionization mass spectrometer with the procedures described by Housh and McMahon [46]. Values have been adjusted to reflect the $^{87}Sr/^{86}Sr$ ratios shifted relative to the difference between the analysis day's values for NBS987 (0.710248) and the accepted value (0.71025).

3. Results

Physio-chemical properties, strontium isotope compositions, and major ion concentrations of water samples are listed in Table 1. Water temperatures are between 26.5 and 32.5 °C. Waters display a circumneutral pHm with values ranging from 7.5 to 7.85, except for site AGA, with a pH value of 8.23. Yalahau region water samples all have total dissolved solid (TDS) values less than 300 mg/L, except for site SAF1 (505.4 mg/L), which showed a significantly higher TDS concentration, similar to that of control points VL and POZO10 (513.7–611.7 mg/L). There is a similar pattern regarding electrical conductivity, where the Yalahau region sites display a range of 120–291 µS/cm, with site SAF1 showing elevated values (481 µS/cm) closer to the control points (496–591 µS/cm).

Table 1. Hydrogeochemical properties, major ions, and strontium isotopic composition of water samples. Units are (mg/L) for all ion geochemistry unless otherwise listed.

Site Name		Location (UTM)	T °C	pH	EC	DO	ORP	HCO_3^-	SO_4^{2-}	Cl^-	Ca^{2+}	Mg^{2+}	K+	Na^+	Sr^{2+}	TDS	$^{87}Sr/^{86}Sr$
Western Yalahau Fracture Zone	CL1	463748.72 2352285.01	28.6	7.67	159.3	2.83	146.3	67.7	0.215	6.439049	30.047	1.824	0.376	3.26	0.1	111.4	0.709046
	SAF1	465700.33 2348530.16	30.9	7.83	481	6.26	107.6	166.3	20.284	119.0887	95.713	32.428	1.939	62.342	0.8	505.4	0.707888
	SAF2	456503.27 2347660.33	32.5	7.74	120.2	3.25	89.6	64	1.029	8.124794	42.241	2.889	2.205	6.535	<0.1	128.7	0.70858
	SPW1	456140.19 2319407.87	29.5	7.56	156.9	2.31	132.3	123.2	3.303	23.05512	85.467	15.323	1.003	14.237	0.4	269.4	0.70836
	SPW2	454049.82 2319652.57	28.7	7.51	240	1.81	99.8	156.5	1.654	15.40646	71.514	11.461	2.239	10.96	0.4	69	0.708175
	VLN	463089.33 2318736.03	29.7	7.56	156.9	2.51	132.3	69	0.976	5.060984	49.568	4.44	3.196	4.19	0.2	138.4	0.708667
Eastern Yalahau Fracture Zone	AGA	466097.06 2306386	28.1	8.23	234	7.3	128.3	103.4	7.072	34.13449	48.096	15.008	1.1916	19.451	0.3	232.3	0.708331
	LVV	471528.2 2317978.6	30.5	7.67	245	2.51	77.5	94.9	6.445	36.92464	40.564	8.119	0.898	13.719	0.3	204.5	0.708515
	NAK	466324.54 2303992.03	28.7	7.83	291	5.79	74.6	102.1	8.752	49.7406	59.55	19.497	0.974	27.574	0.5	272.1	0.708263
	DZIPOZ	490805.17 23458004.94	21.3	7.75	275	4.77	106.6	124.4	2.148	39.3466	34.204	2.303	0.504	8.851	1.16	215.6	0.709103
Control Points	POZO10	500618.52 2332227.56	27.5	7.54	496	5.88	192.8	142.8	31.546	144.3393	83.272	16.045	4.02	83.94	1.14	513.7	0.708976
	VL	493131.22 2306713.65	26.5	7.56	591	2.63	162.3	184.8	26.148	176.0915	112.941	25.131	3.833	74.177	0.7	611.7	0.709667

Water **2020**, *12*, x FOR PEER REVIEW 7 of 15

3.1. Major Ion Geochemistry

3.1. Major Ion Geochemistry

The major ion geochemistry determined two water types within our system. Piper diagrams were used to graphically display and compare geochemical parameters used to determine water types (Figure 2 [47]). The sampling sites exhibit a predominantly Ca^{2+}-HCO_3^- water type, excluding site SAF1. SAF1 and eastern coastal aquifer control points reveal a Ca^{2+}-Mg^{2+}-Cl^- water type.

The major ion geochemistry determined two water types within our system. Piper diagrams were used to graphically display and compare geochemical parameters used to determine water types (Figure 2 [47]). The sampling sites exhibit a predominantly Ca^{2+}-HCO_3^- water type, excluding site SAF1. SAF1 and eastern coastal aquifer control points reveal a Ca^{2+}-Mg^{2+}-Cl^- water type.

Major ion results show three distinct groupings of waters based on geographical location and zonation within the Piper diagram. Three groups were identified: Western Yalahau Fracture Zone (WYFZ), Eastern Yalahau Fracture Zone (EYFZ), and control points (CPP).

Major ion results show three distinct groupings of waters based on geographical location and zonation within the Piper diagram. Three groups were identified: Western Yalahau Fracture Zone (WYFZ), Eastern Yalahau Fracture Zone (EYFZ), and control points (CPP).

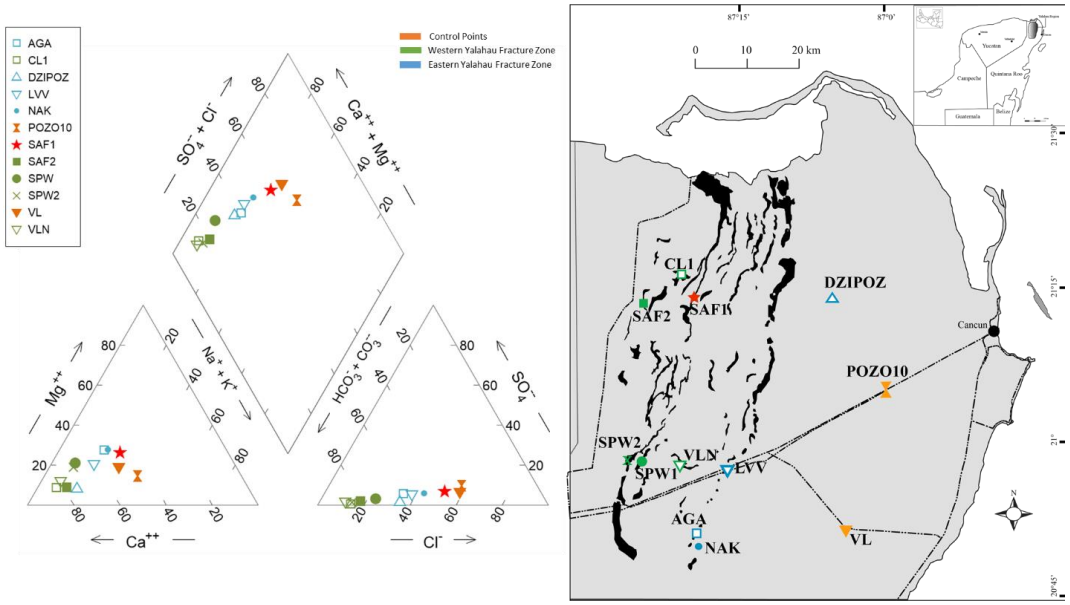

Figure 2. Piper diagram of Yalahau region sites indicating bulk water composition of water samples from sampling sites with adjacent site map. Site symbols correlate to the Piper diagram.

Figure 2. Piper diagram of Yalahau region sites indicating bulk water composition of water samples from sampling sites with adjacent site map. Site symbols correlate to the Piper diagram.

3.2. Control Points (CP)

3.2. Control Points (CP)

The control points (VL, POZO10) display higher concentrations of sulfate and chloride (64–67%) and lower concentrations of bicarbonate and carbonate ions (32–35%). The proportion of sodium (30–40%) is higher than most Yalahau fracture samples and the proportion of calcium (45–51%) is lower. Additionally, control points show higher TDS and EC values than both Western Yalahau Fracture Zone and Eastern Yalahau Fracture Zone samples.

The control points (VL, POZO10) display higher concentrations of sulfate and chloride (64–67%) and lower concentrations of bicarbonate and carbonate ions (32–35%). The proportion of sodium (30–40%) is higher than most Yalahau fracture samples and the proportion of calcium (45–51%) is lower. Additionally, control points show higher TDS and EC values than both Western Yalahau Fracture Zone and Eastern Yalahau Fracture Zone samples.

3.3. Western Yalahau Fracture Zone (WYFZ)

3.3. Western Yalahau Fracture Zone (WYFZ)

The dominant anions in Western Yalahau Fracture Zone samples contain high proportions of bicarbonate and carbonate ions (73–87%) and low proportions of sulfate and chloride (12–27%). Dominant cations in Western Yalahau Fracture Zone samples showed high proportions of calcium (70–74%), magnesium (8–21%), and sodium (8–13%). Physio-chemical properties including temperature, pH, electrical conductivity (EC), dissolved oxygen, and oxidation-reduction potential exist in a normal range. Low EC values imply that saline intrusion is not a factor in the hydrogeochemical process that controls this part of the region. Meanwhile, most of our sites within the Western Yalahau Fracture Zone exhibit similar hydrogeochemical characteristics.

The dominant anions in Western Yalahau Fracture Zone samples contain high proportions of bicarbonate and carbonate ions (73–87%) and low proportions of sulfate and chloride (12–27%). Dominant cations in Western Yalahau Fracture Zone samples showed high proportions of calcium (70–74%), magnesium (8–21%), and sodium (8–13%). Physio-chemical properties including temperature, pH, electrical conductivity (EC), dissolved oxygen, and oxidation-reduction potential exist in a normal range. Low EC values imply that saline intrusion is not a factor in the hydrogeochemical process that controls this part of the region. Meanwhile, most of our sites within the Western Yalahau Fracture Zone exhibit similar hydrogeochemical characteristics.

3.4. Site SAF1

3.4. Site SAF1

Site SAF1 displays similar geochemistry to that of our control points, with higher concentrations of sulfate and chloride (58%) and lower concentrations of bicarbonate and carbonate ions (40%). An

Site SAF1 displays similar geochemistry to that of our control points, with higher concentrations of sulfate and chloride (58%) and lower concentrations of bicarbonate and carbonate ions (40%).

An increase in the proportion of sodium (27%) and a decrease in the proportion of calcium (46%) were observed. During sampling at site SAF1, there were visibly faster flowing waters at the surface when compared to the rest of the Yalahau sampling points. Additionally, control points and site SAF show higher TDS and EC values than both Western Yalahau Fracture Zone and Eastern Yalahau Fracture Zone samples.

3.5. Eastern Yalahau Fracture Zone (EYFZ)

Samples located within the Eastern Yalahau Fracture Zone also exhibit a classification of Ca^{2+}-$HCO3^{-}$ water type, similar to the Western Yalahau Fracture Zone. However, as seen by the zonation of the Eastern Yalahau Fracture Zone within the Piper diagram (Figure 2), it lies closer to the boundary of Ca^{2+}-Mg^{2+}-Cl^{-} mixed type than the Western Yalahau Fracture Zone samples. This is due to elevated proportions of sulfate and chloride (36–48%) compared and more moderate bicarbonate and carbonate ion proportions (51–63%). Magnesium proportions in Eastern Yalahau Fracture Zone sites are slightly higher than in the Western Yalahau Fracture Zone (20–30%). There are no significant anomalies within our Eastern Yalahau Fracture Zone sites in terms of ion geochemistry. Based on zonation within the Piper diagram, site DZIPOZ plots within the Eastern Yalahau Fracture Zone.

3.6. $^{87}Sr/^{86}Sr$

Throughout much of the Yucatán Peninsula, $^{87}Sr/^{86}Sr$ remain constant, varying primarily in the thousands place (e.g., 0.708987; Figure 3). Yalahau waters exhibit similar strontium isotopic ratios in a range of waters throughout the same region (Quintana Roo, Yucatán Peninsula), shown by previous work in the area [6,7]. Water samples in the Yalahau fractures yield $^{87}Sr/^{86}Sr$ values ranging from 0.707888 to 0.709046. Control point samples display slightly higher $^{87}Sr/^{86}Sr$ values than much of the Yalahau waters, with a range of 0.708976–0.709667. Strontium isotopic signatures are plotted in Figure 3 with colors associated with the seawater isotope ratio appropriate for the geologic age of the bedrock with modern seawater being 0.709175 [48].

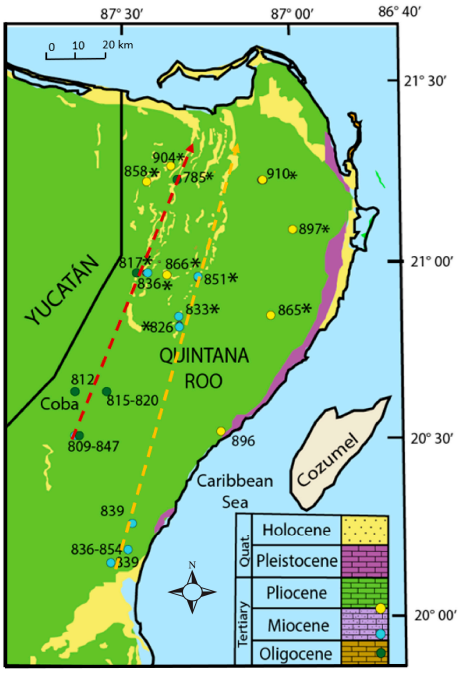

Figure 3. Map showing $^{87}Sr/^{86}Sr$ values (in thousands place) and geology of Yalahau region sites. Southern locations are from a study by Perry et al. [7] while sites with a * are from this study. Red arrow indicates potential path of flow for Western Yalahau Fracture Zone. Orange arrow indicates potential path of flow for Eastern Yalahau Fracture Zone (modified from [7,22]).

4. Discussion

4.1. Hydrogeochemistry

In the Yucatán Peninsula, the slow-moving groundwater will obtain its ion chemistry from abundant minerals in local aquifer rocks—gypsum, calcite, dolomite, and accessory minerals [6,7]. Waters in fast-moving flow systems, such as the Yalahau Fracture Zone, tend to retain the chemical features of its source region [6]. Water moving through these channels is most likely moving fast enough that the interaction between water and aquifer rock is insignificant [7]. Using the Sr isotopic ratio (Figure 3), it can be determined that water flowing through the Yalahau region retains a ratio similar to its southern source region aquifer rock rather than local aquifer bedrock. Under this assumption, this water can be classified as fast moving. All water samples exhibit high proportions of calcium and magnesium (>59%). This is expected due to one of the dominant natural processes that control the hydrochemistry of the Northern Yucatán Peninsula being carbonate weathering, where geochemistry is affected by the dissolution of abundant minerals, $CaCO_3$ (calcite) and $CaMg(CO_3)_2$ (dolomite) [1,49]. In the Eastern Yalahau Fracture Zone, an increase in magnesium content suggests that the Eastern Yalahau Fracture Zone possibly interacts with bedrock dominated by dolostone weathering, while the Western Yalahau Fracture Zone most likely interacts with bedrock dominated by limestone weathering.

Seawater intrusion is widespread throughout much of the Yucatán and reaches up to 100 km inland sitting under a thin freshwater lens [14]. Studies by Tulaczyk [5] did not find evidence for this saline intrusion more than a few kilometers off the eastern coast; however, the ion geochemistry of site SAF1 supports the presence of this intrusion further inland. High chloride values in SAF1 waters may be present for a variety of reasons: (1) a thinner freshwater lens present in the region, (2) an increased mixing of saline water from the seawater intrusion due to a higher flow velocity [6], or (3) the presence of halite in rocks interacting with waters. It is unlikely that the chloride values at site SAF1 are due to the presence of halite, as the source of halite typically comes from evaporite, of whose existence no evidence has been found within the Yalahau region [6,7]. The first two points are explored through observations of the major ion geochemistry and strontium geochemistry of waters throughout the region.

There is a linear relationship between SO_4^{2-} and Na^+ (Figure 4, Table 1). From this, we can attribute the source of sulfate in the waters of SAF1, VL, and POZO10 to seawater. Sulfate is a major component of seawater and its presence is indicative of saltwater intrusion [50] and gypsum. Sites that exhibit higher concentrations of sulfate also indicate higher values of electrical conductivity and total dissolved solids; additionally, these sites are in closer proximity to the coast, excluding site SAF1. These data further support the influence of seawater in the hydrogeochemistry of site SAF1. This influence of seawater can be possibly attributed to a thinner freshwater lens below site SAF1, where the halocline is sitting much higher than in surrounding areas.

Water **2020**, *12*, x FOR PEER REVIEW 10 of 15

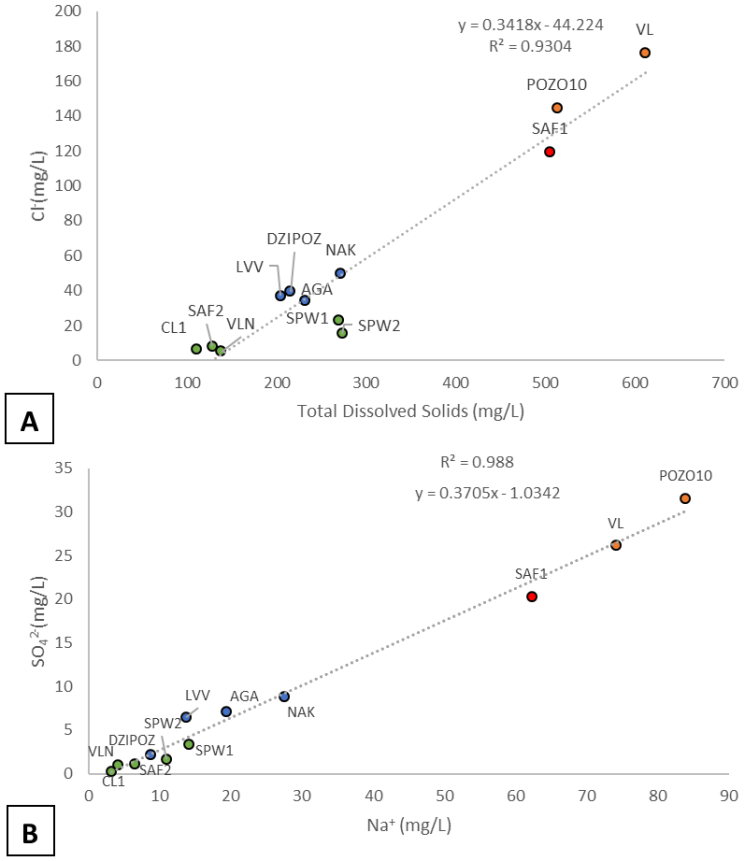

Figure 4. Total dissolved solids/chloride ion and sulfate/sodium plot. (**A**) Chloride/total dissolved solids, (**B**) sodium/sulfate.

4.2. $^{87}Sr/^{86}Sr$

Strontium isotope ratios of Yalahau region sites are plotted on the geology map of the Yucatán Peninsula (Figure 3) alongside strontium isotopic data from the rest of the region [7]. Ratios are also plotted, with color schemes corresponding to the strontium isotopic signature relative to the seawater age curve [48]. While not all Western Yalahau Fracture Zone points conform previous studies [7], we do infer an influx of $^{87}Sr/^{86}Sr$ ratios corresponding to those of Oligocene-age rocks coming through within present study sites and previously studied sites in the western portion of the fracture zone (arrow on Figure 3). This suggests that waters flowing through the Western Yalahau Fracture Zone are more likely to interact with older rocks than waters flowing through the Eastern Yalahau Fracture Zone. In the present study, the Eastern Yalahau Fracture Zone and eastern fracture zone sites from the previous study have $^{87}Sr/^{86}Sr$ ratios different from those of the Miocene age. Many sample sites within the Holbox Fracture Zone, excluding site CL1 and VLN, do not have the same strontium isotopic signature of local aquifer bedrock (Pleistocene or Holocene; Figure 3) [7]. This supports the hypothesis that waters flowing through the Holbox Fracture Zone are flowing through faster channels than much of the Yucatán [6,7]. Identifying the Holbox Fracture Zone waters as being fast flowing, along with further constraining a mixing model, is essential in determining the source of waters in the fracture zone and determining the divide in the various flow paths throughout the zone.

Strontium isotope ratios of Yalahau region sites are plotted on the geology map of the Yucatán Peninsula (Figure 3) alongside strontium isotopic data from the rest of the region [7]. Ratios are also plotted, with color schemes corresponding to the strontium isotopic signature relative to the seawater age curve [48]. While not all Western Yalahau Fracture Zone points conform previous studies [7], we do infer an influx of $^{87}Sr/^{86}Sr$ ratios corresponding to those of Oligocene-age rocks coming through within present study sites and previously studied sites in the western portion of the fracture zone (arrow on Figure 3). This suggests that waters flowing through the Western Yalahau Fracture Zone are more likely to interact with older rocks than waters flowing through the Eastern Yalahau Fracture Zone. In the present study, the Eastern Yalahau Fracture Zone and eastern fracture zone sites from the previous study have $^{87}Sr/^{86}Sr$ ratios different from those of the Miocene age. Many sample sites within the Holbox Fracture Zone, excluding site CL1 and VLN, do not have the same strontium isotopic signature of local aquifer bedrock (Pleistocene or Holocene; Figure 3) [7]. This supports the hypothesis that waters flowing through the Holbox Fracture Zone are flowing through faster channels than much of the Yucatán [6,7]. Identifying the Holbox Fracture Zone waters as being fast flowing, along with further constraining a mixing model, is essential in determining the source of waters in the fracture zone and determining the divide in the various flow paths throughout the zone.

4.3. Sr Endmember Mixing Model

A binary mixing model between two endmembers (A,B) was constructed to examine possible mixing processes in Yalahau waters (Figure 5). Two theoretical mixing lines are displayed. The binary mixing equation was used to create the model [51]:

Water **2020**, *12*, x FOR PEER REVIEW 11 of 15

4.3. Sr Endmember Mixing Model

A binary mixing model between two endmembers (A,B) was constructed to examine possible mixing processes in Yalahau waters (Figure 5). Two theoretical mixing lines are displayed. The binary mixing equation was used to create the model [51]:

$$(^{87}Sr/^{86}Sr)M = (^{87}Sr/^{86}Sr)A\,fa(SrA/SrM) + (^{87}Sr/^{86}Sr)B \times (1 - fa)(SrB/SrM) \quad (1)$$

$$(^{87}Sr/^{86}Sr)M = (^{87}Sr/^{86}Sr)A\,fa(SrA/SrM) + (^{87}Sr/^{86}Sr)B \times (1 - fa)(SrB/SrM) \quad (1)$$

where A and B are endmembers and M is the combination of them. Both lines use site CL1 as theoretical endmember A, due to its location as the most northern site and high $^{87}Sr/^{86}Sr$ ratio, indicating a relatively young age. Mixing model A uses site SPW2 from our suite of samples as endmember B, due to its low $^{87}Sr/^{86}Sr$ ratio and its location within our Yalahau region sites. Mixing model A fails to encompass all sample locations as SAF1 plots outside of endmember B, making it invalid when interpreting the mixing processes of the fracture zone. This suggests that the upper 50 km of the Holbox Fracture Zone interacts and mixes with waters beyond its bounds, likely farther south of the Yalahau region. To account for this, we created a second mixing model using a site farther south of our sites.

where A and B are endmembers and M is the combination of them. Both lines use site CL1 as theoretical endmember A, due to its location as the most northern site and high $^{87}Sr/^{86}Sr$ ratio, indicating a relatively young age. Mixing model A uses site SPW2 from our suite of samples as endmember B, due to its low $^{87}Sr/^{86}Sr$ ratio and its location within our Yalahau region sites. Mixing model A fails to encompass all sample locations as SAF1 plots outside of endmember B, making it invalid when interpreting the mixing processes of the fracture zone. This suggests that the upper 50 km of the Holbox Fracture Zone interacts and mixes with waters beyond its bounds, likely farther south of the Yalahau region. To account for this, we created a second mixing model using a site farther south of our sites.

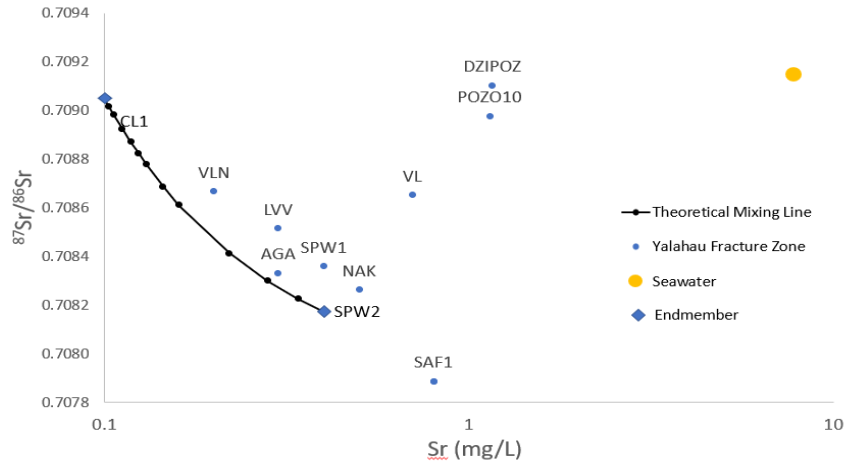

(**A**)

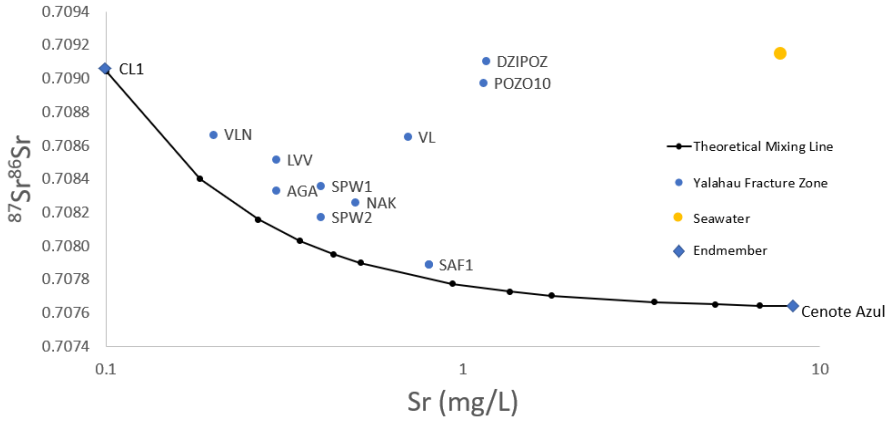

(**B**)

Figure 5. Theoretical mixing line of binary mixing model representing waters from areas in Quintana Roo. **(A) Endmember A is site CL1, endmember B is site SPW2. (B) Endmember A is site CL1 and endmember B is site Cenote Azul** [7].

Mixing model B uses site Cenote Azul [7] as endmember B, due to its far-south location, lower $^{87}Sr/^{86}Sr$ ratio, and its possible preferential flow path into the Holbox Fracture Zone. All Yalahau sites plot within this theoretical mixing model. Most Yalahau sites plot within the first half of the mixing line, signifying that the waters interact with rocks in the more northern region of Quintana Roo. Cenote Azul is most likely too far south to be instrumental in the mixing process that occurs within

Mixing model B uses site Cenote Azul [7] as endmember B, due to its far-south location, lower $^{87}Sr/^{86}Sr$ ratio, and its possible preferential flow path into the Holbox Fracture Zone. All Yalahau sites plot within this theoretical mixing model. Most Yalahau sites plot within the first half of the mixing line, signifying that the waters interact with rocks in the more northern region of Quintana Roo. Cenote Azul is most likely too far south to be instrumental in the mixing process that occurs within the northern portion of the fracture zone. Further Sr data and $^{87}Sr/^{86}Sr$ data need to be collected in groundwater and rocks in sites further south than the Yalahau sites and north of Cenote Azul to further constrain this model. A better constrained model will assist in further determining the extent of the Holbox Fracture Zone's water flow by observing the influence of neighboring waters on the mixing of Holbox Fracture Zone waters. In both of our models, sites DZIPOZ, POZO10, and VL do not plot near the mixing line; instead, they plot closer to the modern seawater point. This is probably because these sites experience the most seawater influence due to their proximity to the Caribbean coast.

5. Conclusions

The flows through the Yalahau region and karst channels are complicated. The waters in this area of the Yucatán flow through fast flowing channels, making the hydrogeology of the area more complex. The major ion geochemistry indicates possible saline intrusion within the fracture zone at least 23 miles off the northern coast and 55 miles off the eastern coast. Results have shown the potential for multiple flow paths to exist within the Holbox Fracture Zone in the Yalahau region. The presence of varying flow paths in the region could have a significant effect on the contaminant risk of municipal water supply that faces north-eastern coastal cities of the Yucatán, including the town of Chiquilá and the increasingly popular tourist destination Isla Holbox. Mixing models suggest that the waters flowing through the Yalahau region in the fracture zone mix with waters further south of the Yalahau. This shows evidence for the extension of the fracture zone beyond visible sabanas.

Over the past 35 years, tourism has increased on the eastern side of the Yucatan Peninsula [52,53]. This rise in tourism has led to a rise in tourism-based developments that have significant effects on the natural ecosystem and local communities. For most of this time, tourism demand has focused on Eastern Yucatán coastal destinations (Cancún, Playa del Carmen); however, within the last 15 years, the northern coast of Yucatan has seen a rapid increase in urban and tourism development of areas in and leading to Holbox Island. The karst fissured porosity, abundance of sabanas, and unknown hydrogeologic characteristics in the Yalahau region raise concern about the possible detrimental effects of development on the region's ecosystem.

Author Contributions: J.M. as lead author wrote the manuscript as part of her MS Thesis at Northern Illinois University. M.L. and R.M.L.-B. edited, analyzed, and advised on the whole article. All authors have read and agreed to the published version of the manuscript.

Funding: This study was funded by the NSF Grant HER-1560045 and the NIU Department of Geology and Environmental Geosciences.

Acknowledgments: This study was funded by the NSF Grant HER-1560045 and the NIU Department of Geology and Environmental Geosciences. Additional support was provided by Philip Carpenter, Josh Schwartz, Anna Buczynska, and Justin Dodd at Northern Illinois University and Kenneth Voglesonger at Northeastern Illinois University. Thank you, reviewers.

Conflicts of Interest: The authors declare no conflict of interest.

References

1. Weidie, A.E. Geology of Yucatan Platform. In *Geology and Hydrogeology of the Yucatan and Quaternary Geology of Northeastern Yucatan Peninsula*; Ward, W.C., Weidie, A.E., Back, W., Eds.; New Orleans Geological Society: New Orleans, LA, USA, 1985.
2. Weidie, A.E. (Ed.) *Lineaments on the Yucatan Peninsula and Fractures of the Central Quintana Roo Coast: Road Log and Supplement to 1978*; Guidebook, Field trip no. 10, Yucatan; Geological Society of America Meeting (GSA): Washington, DC, USA, 1982; pp. 21–25.

3. Southworth, C.S. Applications of remote sensing data, eastern Yucatan. In *Geology and Hydrogeology of the Yucatan and Quaternary Geology of Northeastern Yucatan Peninsula*; Weidie, A.E., Ed.; New Orleans Geological Society: New Orleans, LA, USA, 1985; pp. 12–19.
4. Fedick, S.L.; Morrison, B.A.; Andersen, B.J.; Boucher, S.; Acosta, J.C.; Mathews, J.P. Wetland Manipulation in the Yalahau Region of the Northern Maya Lowlands. *J. Field Archaeol.* **2000**, *27*, 131. [CrossRef]
5. Tulaczyk, S.M. Karst Geomorphology and Hydrogeology of the Northeastern Yucatán Peninsula, Mexico. Master's Thesis, Northern Illinois University, DeKalb, IL, USA, 1993.
6. Perry, E.; Velazquez-Oliman, G.; Marín, L. The Hydrogeochemistry of the Karst Aquifer System of the Northern Yucatan Peninsula, Mexico. *Int. Geol. Rev.* **2002**, *44*, 191–221. [CrossRef]
7. Perry, E.; Paytan, A.; Pedersen, B.; Velazquez-Oliman, G. Groundwater geochemistry of the Yucatan Peninsula, Mexico: Constraints on stratigraphy and hydrogeology. *J. Hydrol.* **2009**, *367*, 27–40. [CrossRef]
8. Gondwe, B.R.N.; Hong, S.-H.; Wdowinski, S.; Bauer-Gottwein, P. Hydrologic Dynamics of the Ground-Water-Dependent Sian Ka'an Wetlands, Mexico, Derived from InSAR and SAR Data. *Wetlands* **2010**, *30*, 1–13. [CrossRef]
9. Solleiro-Rebolledo, E.; Cabadas-Báez, H.; Pi, P.; Gonzalez, A.; Fedick, S.; Chmilar, J.; Leonard, D. Genesis of hydromorphic Calcisols in wetlands of the northeast Yucatan Peninsula, Mexico. *Geomorphology* **2011**, *135*, 322–331. [CrossRef]
10. Fedick, S.L.; Mathews, J.P. The Yalahau regional human ecology project: An introduction and summary of recent research. In *Quintana Roo Archaeology*; Shaw, J.M., Mathews, J.P., Eds.; University of Arizona Press: Tucson, AZ, USA, 2005; pp. 33–50.
11. Glover, J.B. The Yalahau Regional Settlement Pattern Survey: A Study of Ancient Maya Social Organization in Northern Quintana Roo, Mexico. Ph.D. Thesis, University of California, Riverside, CA, USA, 2006.
12. Connors, M.; Hildebrand, A.R.; Pilkington, M.; Ortiz-Aleman, C.; Chávez, R.E.; Urrutia-Fucugauchi, J.; Graniel-Castro, E.; Camara-Zi, A.; Vasquez, J.; Halpenny, J.F. Yucatán karst features and the size of Chicxulub crater. *Geophys. J. Int.* **1996**, *127*, F11–F14. [CrossRef]
13. Rubio-Cisneros, N.; Herrera-Silveira, J.; Morales-Ojeda, S.; Moreno-Báez, M.; Montero, J.; Pech-Cárdenas, M. Water quality of inlets' water bodies in a growing touristic barrier reef Island "Isla Holbox" at the Yucatan Peninsula. *Reg. Stud. Mar. Sci.* **2018**, *22*, 112–124. [CrossRef]
14. Bauer-Gottwein, P.; Gondwe, B.R.N.; Charvet, G.; Marín, L.E.; Rebolledo-Vieyra, M.; Merediz-Alonso, G. Review: The Yucatán Peninsula karst aquifer, Mexico. *Hydrogeol. J.* **2011**, *19*, 507–524. [CrossRef]
15. Reeve, A.; Perry, E.C. Hydrogeology and tidal analysis along the western north coast of the Yucatan Peninsula, Mexico. In *Tropical Hydrology and Caribbean Water Resources: Proceedings of the International Symposium on Tropical Hydrology and Fourth Caribbean Islands Water Resources Congress, San Juan, PR, USA, 22–27 July 1990*; Krishna, J.H., Ed.; American Water Resources Association: Bethesda, MD, USA, 2000; pp. 327–337.
16. Perry, E.C.; Velazquez-Oliman, G.; Socki, R. The hydrogeology of the Yucatan Peninsula. In *Hydrogeology of the Yucatan Peninsula, 21st Symposium on Plant Biology*; Pompa, A.G., Fedick, S., Eds.; The Haworth Press: Binghamton, NY, USA, 2001.
17. Beddows, P.A.; Smart, P.L.; Whitaker, F.F.; Smith, S.L. Decoupled fresh-saline groundwater circulation of a coastal carbonate aquifer: Spatial patterns of temperature and specific electrical conductivity. *J. Hydrol.* **2007**, *346*, 18–32. [CrossRef]
18. Supper, R.; Motschka, K.; Ahl, A.; Bauer-Gottwein, P.; Gondwe, B.; Alonso, G.M.; Römer, A.; Ottowitz, D.; Kinzelbach, W. Spatial mapping of submerged cave systems by means of airborne electromagnetics: An emerging technology to support protection of endangered karst aquifers. *Near Surf. Geophys.* **2009**, *7*, 613–627. [CrossRef]
19. Gondwe, B.R.N.; Ottowitz, D.; Supper, R.; Motschka, K.; Merediz-Alonso, G.; Bauer-Gottwein, P. Regional-scale airborne electromagnetic surveying of the Yucatan karst aquifer (Mexico): Geological and hydrogeological interpretation. *Hydrogeol. J.* **2012**, *20*, 1407–1425. [CrossRef]
20. Mongelli, G.; Monni, S.; Oggiano, G.; Paternoster, M.; Sinisi, R. Tracing groundwater salinization processes in coastal aquifers: A hydrogeochemical and isotopic approach in the Na-Cl brackish waters of northwestern Sardinia, Italy. *Hydrol. Earth Syst. Sci.* **2013**, *17*, 2917–2928. [CrossRef]
21. Cary, L.; Benabderraziq, H.; Elkhattabi, J.; Gourcy, L.; Parmentier, M.; Picot, J.; Khaska, M.; Laurent, A.; Négrel, P. Tracking selenium in the Chalk aquifer of northern France: Sr isotope constraints. *Appl. Geochem.* **2014**, *48*, 70–82. [CrossRef]

22. Servicio Geológico Mexicano (SGM). Carta Geológico-Minera, Estados de: Campeche, Quintana Roo y Yucatán, escala 1:500000: 1 mapa. 2017. Available online: www.coremisgm.gob.mx (accessed on 1 May 2020).
23. Moore, Y.H.; Stoessell, R.K.; Easley, D.H. Fresh-Water/Sea-Water Relationship Within a Ground-Water Flow System, Northeastern Coast of the Yucatan Peninsula. *Ground Water* **1992**, *30*, 343–350. [CrossRef]
24. Perry, E.C.; Velazquez-Oliman, G. The hydrogeology of the northern Yucatan Peninsula, Mexico, with special reference to coastal processes. In *Ground Water Discharge in the Coastal Zone: Proceedings of an International Symposium*; Buddemeier, R.W., Ed.; LOICZ (Land Ocean Interactions in the Coastal Zone): Den Burg, The Netherlands, 1996; pp. 92–97.
25. Neumann, K.; Dreiss, S. Strontium 87/strontium 86 rations as tracers in groundwaters and surface waters in Mono Basin, California. *Water Resour. Res.* **1995**, *23*, 3183–3193. [CrossRef]
26. Katz, B.G.; Bullen, T.D. The combined use of 87Sr/86Sr and carbon and water isotopes to study the hydrogeochemical interaction between groundwater and lakewater in mantled karst. *Geochim. Cosmochim. Atca* **1996**, *60*, 5075–5087. [CrossRef]
27. Dogramaci, S.; Herczeg, A.L. Strontium and carbon isotope constraints on carbonate-solution interactions and inter-aquifer mixing in groundwaters of the semi-arid Murray Basin, Australia. *J. Hydrol.* **2002**, *262*, 50–67. [CrossRef]
28. Frost, C.D.; Toner, R.N. Strontium Isotopic Identification of Water-Rock Interaction and Ground Water Mixing. *Ground Water* **2004**, *42*, 418–432. [CrossRef]
29. Negrel, P.; Petelet-Giraud, E.; Widory, D. Strontium isotope geochemistry of alluvial groundwater: A tracer for groundwater resources characterisation. *Hydrol. Earth Syst. Sci.* **2004**, *8*, 959–972. [CrossRef]
30. Wang, Y.; Guo, Q.; Su, C.; Ma, T. Strontium isotope characterization and major ion geochemistry of karst water flow, Shentou, northern China. *J. Hydrol.* **2006**, *328*, 592–603. [CrossRef]
31. Shand, P.; Love, A.J.; Darbyshire, D.P.F.; Edmunds, W.M. Sr isotopes in natural waters: Applications to source characterization and water–rock interaction in contrasting landscapes. In *Water-Rock Interaction*; Bullen, T.D., Wang, Y., Eds.; Taylor and Francis: London, UK, 2007; pp. 27–35.
32. Beddows, P.A. Groundwater Hydrology of a Coastal Conduit Carbonate Aquifer: Caribbean Coast of the Yucatán Peninsula, México. Ph.D. Thesis, University of Bristol, Bristol, UK, 2004.
33. Peterman, Z.E.; Wallin, B. Synopsis of strontium isotope variations in groundwater at Äspö, southern Sweden. *Appl. Geochem.* **1999**, *14*, 939–951. [CrossRef]
34. Curtis, J.B., Jr.; Stueber, A.M. Sr/Sr Ratios and Toal Strontium Concentrations in Surface Waters of the Scioto River Drainage Basin, Ohio. *Ohio J. Sci.* **1973**, *73*, 166–175.
35. Santoni, S.; Huneau, F.; Garel, E.; Aquilina, L.; Vergnaud-Ayraud, V.; Labasque, T.; Celle-Jeanton, H. Strontium isotopes as tracers of water-rocks interactions, mixing processes and residence time indicator of groundwater within the granite-carbonate coastal aquifer of Bonifacio (Corsica, France). *Sci. Total. Environ.* **2016**, *573*, 233–246. [CrossRef] [PubMed]
36. Glover, J.B.; Rissolo, D.; Mathews, J.P. The Hidden World of the Maritime Maya: Lost Landscapes along the North Coast of Quintana Roo, Mexico. In *The Archaeology of Maritime Landscapes*; Ford, B., Ed.; Springer: New York, NY, USA, 2011; Volume 2, pp. 195–216.
37. SEMARNAT. 2019. Available online: http://dgeiawf.semarnat.gob.mx:8080/ibi_apps/WFServlet?IBIF_ex=D3_AGUA01_01&IBIC_user=dgeia_mce&IBIC_pass=dgeia_mce&NOMBREENTIDAD=*&NOMBREANIO=* (accessed on 5 August 2020).
38. Jáuregui, E. Climatology and landfalling hurricanes and tropical storms in Mexico. *Atmósfera* **2003**, *16*, 193–204.
39. Hodell, D.; Brenner, M.; Curtis, J.H. Climate and cultural history of the Northeastern Yucatan Peninsula, Quintana Roo, Mexico. *Clim. Chang.* **2007**, *83*, 215–240. [CrossRef]
40. Beddows, P.A. An Introduction to the Yucatan Peninsula Hydrogeology: A World Class Example of a Coastal Carbonate Density Stratified Aquifer. In *Cavern Guide Training Program*; Asociación de Prestadores de Servícios Acuáticos: Riviera Maya, Mexico, 2003.
41. Perry, E.; Marin, L.; McClain, J.; Velazquez, G. Ring of Cenotes (sinkholes), northwest Yucatan, Mexico: Its hydrogeologic characteristics and possible association with the Chicxulub impact crater. *Geology* **1995**, *23*. [CrossRef]
42. López-Ramos, E. Estudio geológico de la península de Yucatán. In *Boletín de la Asociación Mexicana de Geólogos Petroleros*; Asociación Mexicana de Geólogos Petroleros: San Bartolo, Mexico, 1973; Volume 25, pp. 23–76.

43. Schönian, F.; Tagle, R.; Stöffler, D.; Kenkmann, T. Geology of Southern Quintana Roo (Mexico) and the Chicxulub Ejecta Blanket. In Proceedings of the 36th Lunar and Planetary Science Conference, League City, TX, USA, 14–18 March 2005; p. 2389. Available online: http://www.liber-lapidum.net/frank/frank.html (accessed on 1 May 2020).
44. CONAGUA. *Determinación de La Disponibilidad Del Agua En El Acuífero de La Península de Yucatán [Determination of the Water Availability at the Yucatan Peninsula Aquifer]*; CONAGUA: Ciudad de México, México, 2002; pp. 1–20.
45. Rebolledo-Vieyra, M.; Urrutia-Fucugauchi, J.; Trejo-Garcia, A.; Marin, L.; Sharpton, V.; Soler, A. UNAM's Scientific Shallow Drilling Program into the Chicxulub impact crater. *Int. Geol. Rev.* **2000**, *42*, 928–940. [CrossRef]
46. Housh, T.; McMahon, T.P. Sr, Nd and Pb Isotopic Characteristics of Late Miocene Pleistocene Collision-Related Igneous Rocks in Western New Guinea (Irian Jaya, Indonesia). *Lithos* **2000**, *50*, 217–222.
47. Ghosh, M.J.; Padhy, P.K. Characterization and Classification of Hydrochemistry using Mulitvariate Graphical and Hydrostatistical Techniques. *Res. J. Chem. Sci.* **2013**, *3*, 32–42.
48. McArthur, J.M.; Howarth, R.J.; Bailey, T. Strontium Isotope Stratigraphy: LOWESS Version 3: Best Fit to the Marine Sr-Isotope Curve for 0–509 Ma and Accompanying Look-up Table for Deriving Numerical Age. *J. Geol.* **2001**, *109*, 155–170. [CrossRef]
49. Han, G.; Liu, C.-Q. Water geochemistry controlled by carbonate dissolution: A study of the river waters draining karst-dominated terrain, Guizhou Province, China. *Chem. Geol.* **2004**, *204*, 1–21. [CrossRef]
50. Fitts, C.R. *Groundwater Science*, 2nd ed.; Elsevier: Amsterdam, The Netherlands, 2013.
51. Faure, G.; Mensing, T.M. *Isotope Principle and Applications*, 3rd ed.; John Wiley & Sons: Hoboken, NJ, USA, 2005.
52. Tran, K.C.; Valdés, D.; Euan, J.; Real, E.; Gil, E. Status of water quality at Holbox Island, Quintana Roo State, Mexico. *Aquat. Ecosyst. Heal. Manag.* **2002**, *5*, 173–189. [CrossRef]
53. Leal-Bautista, R.M.; Lenczewski, M.; Morgan, C.; Gahala, A.; McLain, J.E.; Ma., L.-B.R.; Melissa, L.; Cheyenne, M.; Gahala, A.; McLain, J.E. Assessing Fecal Contamination in Groundwater from the Tulum Region, Quintana Roo, Mexico. *J. Environ. Prot.* **2013**, *4*, 1272–1279. [CrossRef]